



**HAL**  
open science

## Blistering phenomenon of molten glass in contact with zirconia-based refractories

J. Hell, P. Vespa, I. Cabodi, O. Citti, F. Fournet-Fayard, J. Fouletier, M.C. Steil

► **To cite this version:**

J. Hell, P. Vespa, I. Cabodi, O. Citti, F. Fournet-Fayard, et al.. Blistering phenomenon of molten glass in contact with zirconia-based refractories. *Journal of the European Ceramic Society*, 2021, 41 (10), pp.5359-5366. 10.1016/j.jeurceramsoc.2021.03.063 . hal-04755060

**HAL Id: hal-04755060**

**<https://hal.science/hal-04755060v1>**

Submitted on 13 Nov 2024

**HAL** is a multi-disciplinary open access archive for the deposit and dissemination of scientific research documents, whether they are published or not. The documents may come from teaching and research institutions in France or abroad, or from public or private research centers.

L'archive ouverte pluridisciplinaire **HAL**, est destinée au dépôt et à la diffusion de documents scientifiques de niveau recherche, publiés ou non, émanant des établissements d'enseignement et de recherche français ou étrangers, des laboratoires publics ou privés.



Distributed under a Creative Commons Attribution - NonCommercial 4.0 International License

## **Blistering phenomenon of molten glass in contact with zirconia-based refractories**

J. Hell<sup>a, b</sup>, P. Vespa<sup>a</sup>, I. Cabodi<sup>a</sup>, O. Citti<sup>a</sup>, F. Fournet-Fayard<sup>b</sup>, J. Fouletier<sup>b</sup>, M.C. Steil<sup>b\*</sup>

<sup>a</sup> SEFPRO SGR Provence, F-84306 Cavaillon Cedex

<sup>b</sup> Univ. Grenoble Alpes, Univ. Savoie Mont Blanc, CNRS, Grenoble INP, LEPMI, 38 000, Grenoble, France

\*Corresponding author

*KEYWORDS: blistering, oxygen semipermeation, refractories, zirconia percolation, redox state*

---

### ABSTRACT:

The contact between a glass melt and some refractories in glass industry is able to induce a blistering phenomenon, **which is detrimental for obtaining high quality glasses**. The objective of this study is to define the key parameters of the blistering process and to propose a mechanism for blistering of soda–lime–silica glass melts in contact with fused-cast zirconia-based refractories. The roles of oxygen semipermeability through the zirconia skeleton and of temperature are emphasized.

---

### Introduction

During the glass fabrication process, the contact between refractories and molten glass is sometimes subject to blistering phenomena: in addition to the release of few gases trapped in the closed porosity of the refractory, redox processes in glass and refractories can result in the production of gas. This blistering phenomenon occurs at different levels of intensity, depending on the glass/refractory couple, on the external conditions, i.e., temperature,

atmosphere, and on the thermal and chemical history, i.e., fining level, redox state of the refractories and of the glass, etc. The formation of gas bubbles is not acceptable in high-quality glasses, both aesthetically and functionally. The first generation of materials for refractory linings in glass melting furnaces, referred to as AZS ( $\text{Al}_2\text{O}_3$  (ca. 45 wt.%) –  $\text{ZrO}_2$  (ca. 35 wt.%) –  $\text{SiO}_2$  (ca. 20 wt.%)), contained high amounts of alumina [1]. However, glass contamination by refractory material dissolution produces defects in the final product. The necessity of producing large amounts of high-purity glasses, such as glasses for flat LCD devices or plasma display panel (PDP) screens, led to the development of refractory materials referred to as High Zirconia Fused-Cast (HZFC) refractories. Owing to their good resistance to corrosion and high temperatures, zirconia-based refractories are, presently, widely used for building furnaces in case of production of glasses high-quality [2]. In order to limit the blistering phenomenon, it is crucial to understand the different parameters playing a role in the phenomenon. Many studies have already been performed in the last 45 years to understand the blistering phenomenon, whether it be on fused-cast zirconia-based refractories or on sintered zircon products. However, very few reports on these studies can be found in the open literature [3–5] and the proposed blistering mechanisms concern either dense zircon ( $\text{ZrSiO}_4$ ) [3, 6], or AZS fused-cast refractories.

The objective of this paper is to provide a better insight on the blistering phenomenon of glasses in contact with high-zirconia fused-cast refractories, referred to as HZFC in the following, at temperatures below the phase transition of zirconia, using specific set-ups. For the first time, it is demonstrated that with fused-cast refractories, the blistering phenomenon at the glass/refractory interface is ascribed to oxygen semipermeation through the refractory material.

## 2. Experimental

## 2.1. Studied material and characterization

High-zirconia fused-cast refractories are obtained by electrofusion: the raw materials are melted at 2250°C with electric energy created between graphite electrodes. The studied fused-cast product contains 91 wt.% ZrO<sub>2</sub> and 9 wt.% of a vitreous phase, referred to as “vph” composed of SiO<sub>2</sub>, Al<sub>2</sub>O<sub>3</sub>, Na<sub>2</sub>O and B<sub>2</sub>O<sub>3</sub>. The microstructure of HZFC refractories consists of monoclinic zirconia embedded in a three-dimensional interconnected amorphous phase, with a glass transition temperature generally around 800 °C [7]. The amorphous phase is crucial, as it increases the viscoplasticity of the refractory material and, hence, accommodates the large volume expansion (ca. 5 %) corresponding to the tetragonal to monoclinic transition of zirconia during the cooling step of the refractory, but also similar contraction during heating-up to reach the service temperature in the industrial furnace. The chemical composition of the vitreous phase is a key factor: its viscosity has to be low enough during zirconia phase transition, thanks to a suitable glass transition temperature. The cooling process is, also, a critical step in the fabrication process, that strongly influences the quality of the final product and has been widely studied [8,9].

The tested refractory was either raw (“as-made material”) with a grey colour or studied after thermal treatment under air at high temperature (1350°C/30h), with a flesh-colour. The tested glass is an industrial soda-lime-silicate glass provided by Saint-Gobain Glass. The AKM glass contains high amounts of alkaline oxides (Na<sub>2</sub>O + K<sub>2</sub>O ~ 15-22 wt.%), alkali-earth oxides (MgO + CaO > 5 wt.%) and also alumina (Al<sub>2</sub>O<sub>3</sub> > 8 wt.%). Minute levels of iron (0.1wt.%) present in the raw powders, segregate in the vitreous phase during the fabrication process of the refractories. The pellets or crucibles studied were cut from internal parts of large blocks.

X-ray diffraction (XRD) characterizations were carried out on a diffractometer PANalytical X'PERT Pro MPD (Cu K<sub>α</sub> radiation: 0.15419 nm). The microstructure of the refractory

materials was investigated by Scanning Electron Microscopy (SEM) images, with a SEM FEG JEOL IT500HR equipped with an energy dispersive X-ray spectrometer (EDX).

The 3D connectivity of the phases (zirconia and vitreous phase) in the refractory was studied by tomography measurements with the EASYTOM XL Nanofoyer. Samples from 1 mm in diameter were characterized with a resolution of 1  $\mu\text{m}$  voxel size.

The redox state of the refractory and of the glass is key parameter in glass industry [6]. The oxidation states of the sample were characterized by measuring the redox state of the iron by X-ray Absorption Near Edge Structure (XANES) experiments performed at the European Synchrotron Radiation Facility (ESRF) – beamline BM30B, in Grenoble (France). *Ex situ* tests were performed, at ambient temperature, in fluorescence mode. The analysis spots were a 200 x 200  $\mu\text{m}^2$  area, involving both vitreous phase zones and  $\text{ZrO}_2$  grains (see Figure 4 (a)). In order to consider that metallic iron might also be present in these materials, a “linear combination fitting” tool available in the software Athena [10] was used, with a set of 12 different references ranking from metallic iron to  $\text{Fe}^{3+}$  based compounds.

## 2.2. Electrical conductivity of the refractory vs. oxygen partial pressure

Impedance spectroscopy was carried out with a symmetric cell under controlled atmosphere in a furnace able to reach 1500°C. The samples were in the form of cylinders (8 mm in diameter, and 6 mm in thickness). The samples were pre-treated at 1350°C for 30 hours under air. Both surfaces were coated with Pt paste (Pt ink 6926, Metalor), dried and fired at 1000 °C for 2 hours. The measurements were carried out with a 1260 Solartron frequency analyzer in the 0.1 – 10<sup>7</sup> Hz frequency range. The gas flowing the cell was pure oxygen, synthetic air, argon, or argon-hydrogen (5%), with a flow rate of 6 L/h. The oxygen partial pressure in argon and argon-hydrogen was controlled and monitored with a zirconia

oxygen pump-sensor device [11,12]. Thus, the oxygen partial pressure can be controlled between 1 and  $10^{-25}$  atm.

### 2.3. Oxygen semipermeability measurements

By using a specific set-up previously developed, schematized in Figure 1, the oxygen semipermeability flux through the refractories has been measured [13-16]. The set-up was modified to reach temperatures up to 1500°C. Owing to the high temperature and the chemical reactivity of the vitreous phase of the refractory, it was not possible to measure the oxygen activity on the membrane surface with point electrodes as made in previous works [13, 15, 17, 18]. A pellet of the studied refractory, pre-treated under air at 1350°C for 30 hours, with a 19 mm diameter, was pressed between two alumina tubes. The gas-tightness was achieved by platinum O-rings. This cell was placed inside another alumina tube to create a guard-chamber with argon flow in order to limit the impact of eventual leakages. An oxygen partial pressure difference was created between the surfaces of the refractory material, i.e., an atmosphere rich in oxygen (0.2 bar) on one side and an argon atmosphere (less than  $10^{-5}$  bar) on the other side. The oxygen pressures upstream ( $P_1$ ) and downstream ( $P_2$ ) the cell were measured precisely using zirconia oxygen sensors [19, 20].

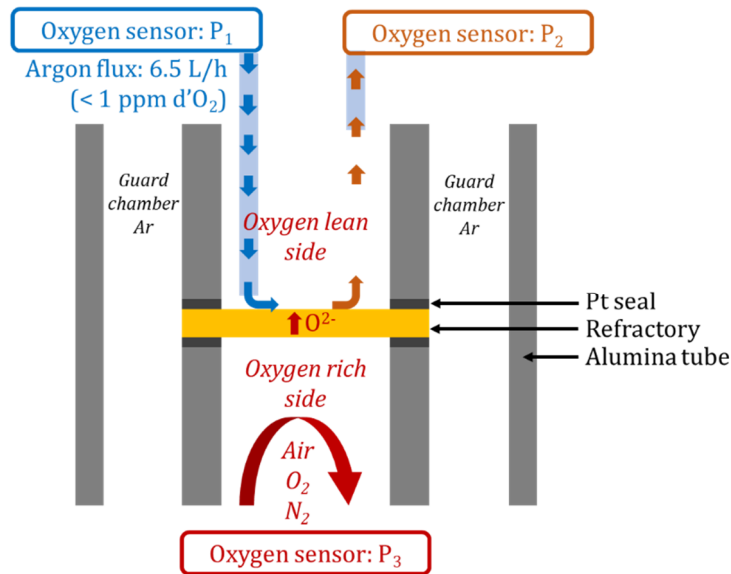


Figure 1: Semipermeability set-up in gas | refractory | gas configuration.

For *in situ* study of the blistering process, the semipermeability set-up was modified. As shown in Figure 2, the membrane was replaced by a crucible (19 mm in external diameter and 25 mm in height). Solid glass was introduced in the crucible before heating the cell (around 5 mm thick). The applied procedure is the following: heat at 100°C/h, from ambient temperature up to 1100°C with argon flowing in all the set-up, then air flux is applied in the chamber below the crucible for the blistering test. A control of the gas-tightness is always done at 820°C. The oxygen pressure on the rich side was generally 0.2 bar, but can be controlled and monitored in the range 1 bar – 10<sup>-5</sup> bar, using a zirconia pump-sensor device (referred to as P<sub>3</sub>). The emf of the zirconia sensor (P<sub>2</sub>), downstream the cell was recorded continuously as shown in Figure 2. Each peak corresponds to one (or several) bubble(s) exploding on the surface of the molten glass and increasing the oxygen concentration in the flowing argon.

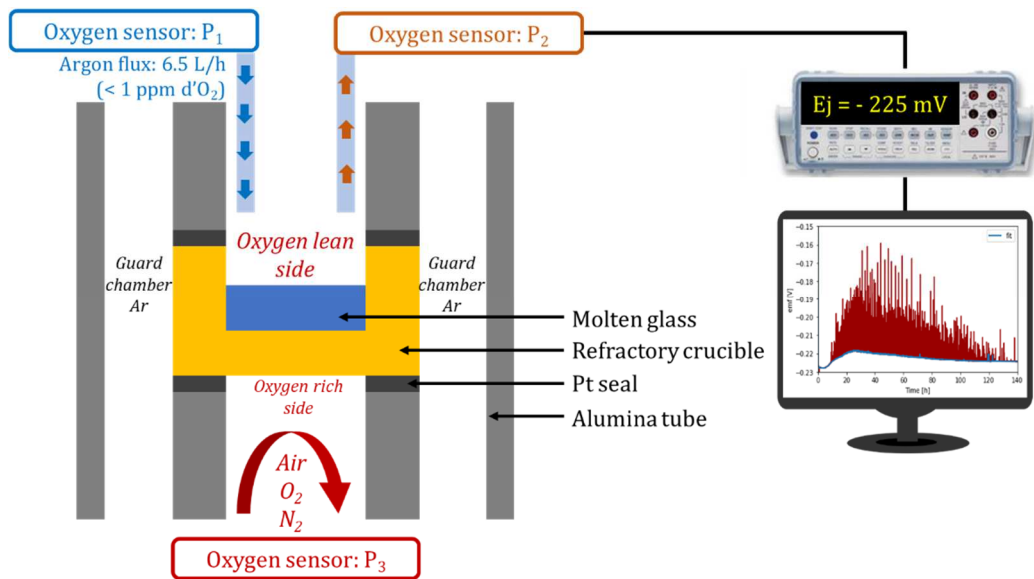


Figure 2: Semipermeability set-up to study the blistering process in a glass in contact with a refractory.

### 3. Results and discussion

#### 3.1. Physical-chemistry Characterization

Various characterizations were made on the as-made refractory or after annealing under air. The objective was to follow the evolution of the refractory in terms of microstructure and chemical composition before the blistering tests.

Figure 3 shows the XRD patterns of an as-made HZFC sample and after oxidation treatment under air, at 1350°C for 30 h. No shift of the peaks characterizing the monoclinic phase was observed after oxidation. However, additional peaks corresponding to the precipitation of traces of zircon ( $\text{ZrSiO}_4$ ) and  $\text{SiO}_2$  can be identified.  $\text{ZrSiO}_4$  results from a chemical reaction between zirconia and the vitreous phase.

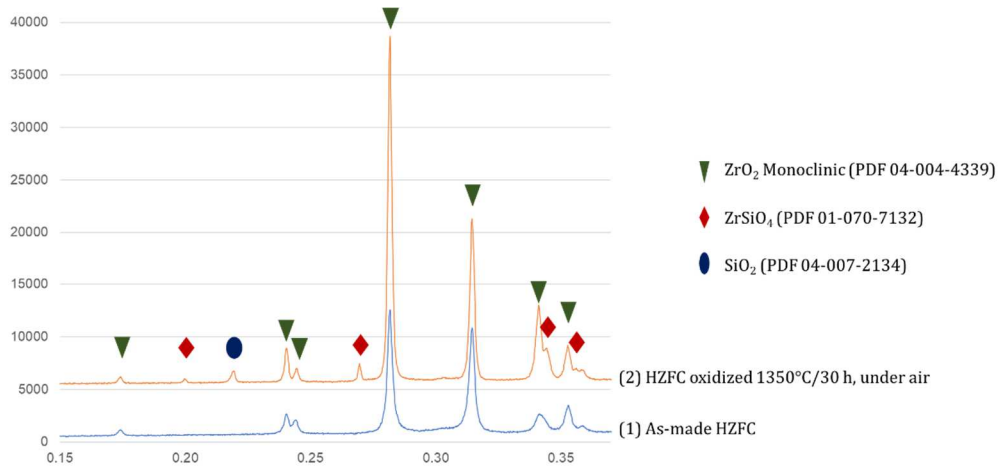


Figure 3: (a): XRD diffractogram of HZFC refractory ((1): As-made HZFC refractory, (2): HZFC refractory oxidized under air at 1350°C/30 h).

The microstructure of the studied refractory was characterized by scanning-electron microscopy. The grain size of zirconia phase was in the range 40 – 150  $\mu\text{m}$ . SEM images of both samples, i.e., as-made and oxidized, (Figures 4 a and b) reveal that most of the monoclinic zirconia grains are surrounded by a thin layer (generally less than 2  $\mu\text{m}$  thick) of the vitreous phase. However, direct contact between zirconia grains is also observed.

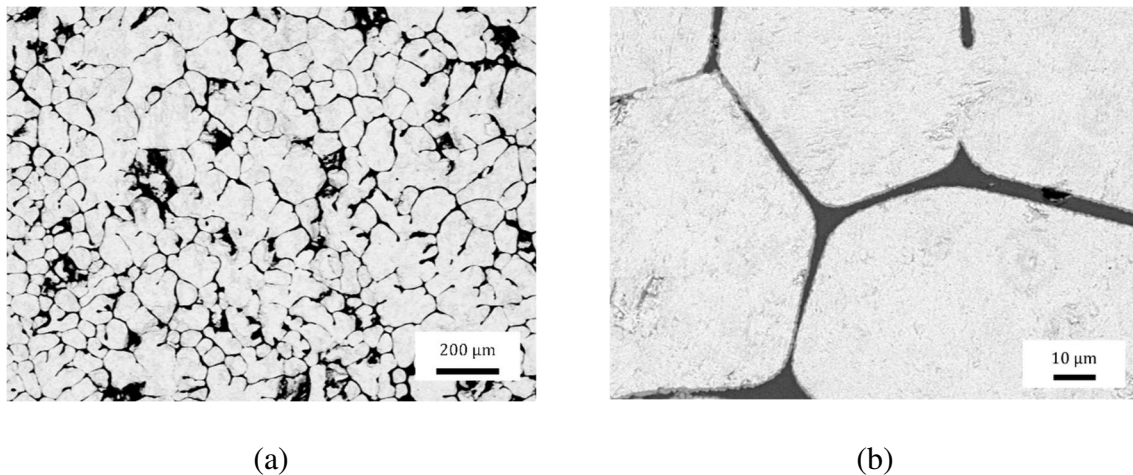


Figure 4: SEM micrographs of the studied HZFC (a) As-made HZFC refractory, (b) HZFC refractory after oxidation under air (1350°C / 30 h) (zirconia phase in grey and vitreous phase in black)

It will be demonstrated in Section 3.3 that the oxygen flux, responsible of the blistering phenomenon, proceeds through the zirconia grains. On the contrary, the vitreous phase, which is a cationic conductor, prevents the oxygen flux occurring. Then, the connectivity of the zirconia phase, within the refractory, was studied by 3-dimensional reconstruction using X-ray absorption tomography. As shown in Figure 5, the zirconia phase is well distributed within the bulk, leading to the percolation of zirconia. The connectivity of the zirconia phase has been considered as responsible of the mechanical properties of the HZFC refractories, such as high creep resistance at high temperature, or elastic stiffness [7]. It can be also concluded that, in the highly-doped zirconia refractory, the zirconia phase is a possible path for oxygen to be transferred from one side of the sample to the other.

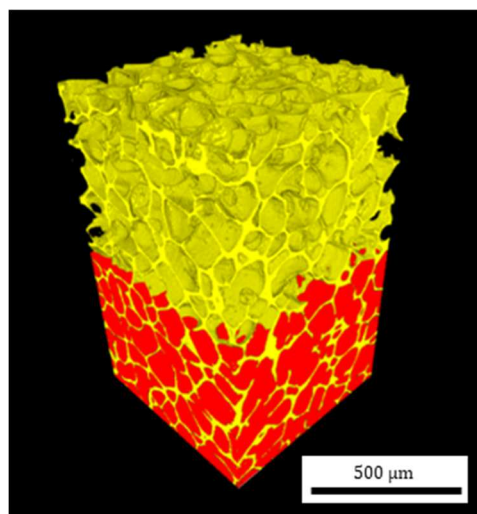


Figure 5: 3D microstructure of the refractory obtained by X-ray absorption tomography of HZFC (zirconia grains in red and glassy phase in yellow).

The redox state of iron of the studied refractory as-made and after controlled heat treatment was characterized by XANES experiments. As shown in Figure 6, after heat treatment (10 hours) under air at 1100°C, a partial oxidation of the pellet was obtained. It should be noted that in the oxidized **flesh-coloured** zones, no more metallic iron was observed since FeO and

$\text{Fe}_2\text{O}_3$ , represent, respectively, 22 wt.% and 78 wt.%. Obviously, different iron oxidation states within the refractory are achieved depending on the treatment atmosphere, on the temperature and on the treatment duration. One can also assume that the color of the high zirconia fused-cast refractories (from dark grey to orange) is indicative of the iron oxidation state. To obtain a complete oxidation of the studied refractory, a heat treatment at 1350°C for 30 h, under air, was carried out before blistering test.

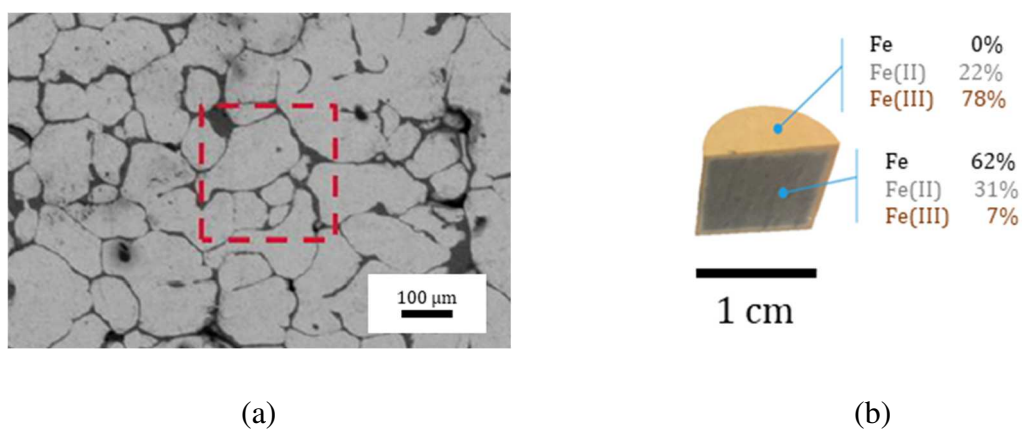


Figure 6: XANES analysis of the HZFC refractory at ESRF, Grenoble. (a) Analysis spot: 200x200  $\mu\text{m}^2$  area, (b) Redox states of iron after heat treatment (10 hours, at 1100°C, under air).

SEM observation shows that iron particles are mainly localized in the vitreous phase (Figure 7): less than 10 % of iron nodules is precipitated within the zirconia phase.

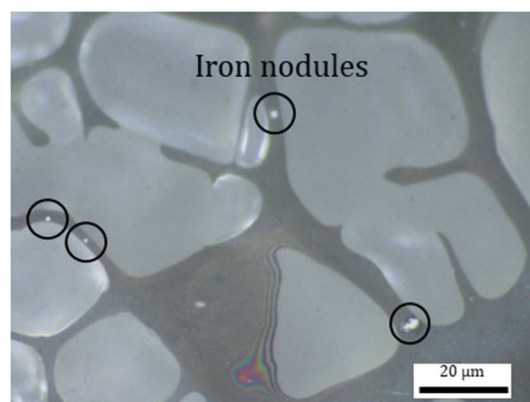
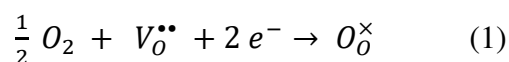


Figure 7: SEM observation of iron nodules in the glassy phase of the as-made HZFC refractory

The oxidation of iron particles within the refractory can be explained by the high temperature metallic corrosion concept [21]. The vitreous phase is an ionic conductor avoiding oxygen transport. The oxygen transport involves exclusively the zirconia phase ( $ZrO_{2-x}$ ) which is a mixed ionic-electronic conductor at high temperature (through oxygen vacancies and electrons). If we consider an iron particle precipitated at the interface between the vitreous phase and a zirconia grain, a simplified oxidation mechanism can be described in three steps, using Kröger-Vink notation (see Figure 8):

1. At the external interface (refractory/air interface): oxygen reduction, referred to as “external half-reaction”:



2. At the internal interface (refractory/iron particle interface): iron oxidation, referred to as “internal half-reaction”:



3. Diffusion of oxygen vacancies and electrons through monoclinic zirconia.

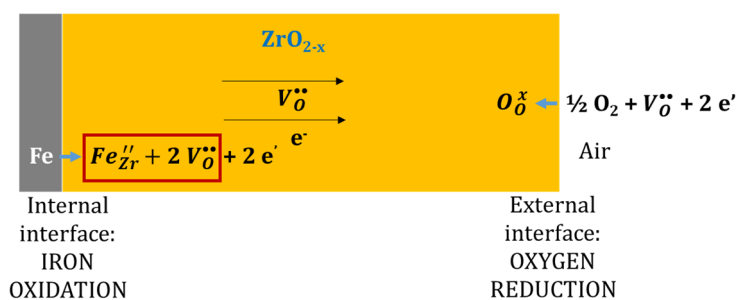


Figure 8: Simplified mechanism of the oxidation of an iron particle in contact with a zirconia grain.

### 3.2. Transport properties of the refractories

Figure 9 gives examples of impedance diagrams of the HZFC refractory, at 1100°C, under three oxygen partial pressures ( $pO_2$ ), i.e., 1 bar, 0.2 bar, and  $10^{-5}$  bar. The separation

between the sample response and the electrode contribution is easy and it can be observed that the total sample resistance ( $R_{tot}$ ) increases as the  $pO_2$  decreases. The total conductivity of the material ( $\sigma_{tot}$ ) can be calculated from the  $R_{tot}$  values and the geometrical factor of the sample.

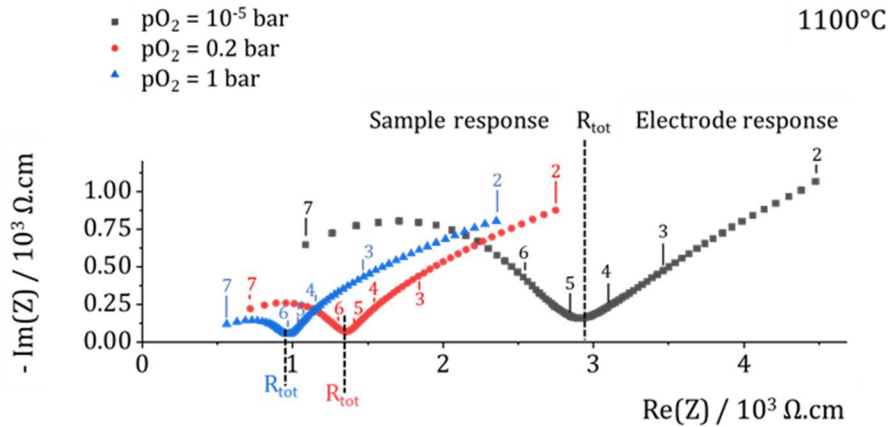


Figure 9: Nyquist diagram of the HZFC refractory, at 1100°C under three oxygen partial pressures. The numbers 1, 2, etc. indicate the  $\log_{10}$  of the measuring frequency.

Figure 10 shows the variation of the total electrical conductivity of HZFC refractory as a function of the oxygen partial pressure, at 1100°C, referred to as a Patterson diagram [22, 23]. The plot is characteristic of a mixed ionic-electronic conductor: under oxygen partial pressures lower than  $10^{-5}$  bar, the conductivity plateau indicates that the material can be considered as a purely ionic conductor, whereas, at high oxygen pressure an additional p-type electronic conductivity is observed. **The conductivity plateau can be ascribed to intrinsic defects (either oxygen vacancies or oxygen interstitials [24]) or impurities (oxides with a valence of the cation lower than 4, such as CaO or  $Y_2O_3$ ) [25,26]. In any case, according to previously published results, the additional electronic conductivity can be ascribed to monoclinic zirconia [27–30].**

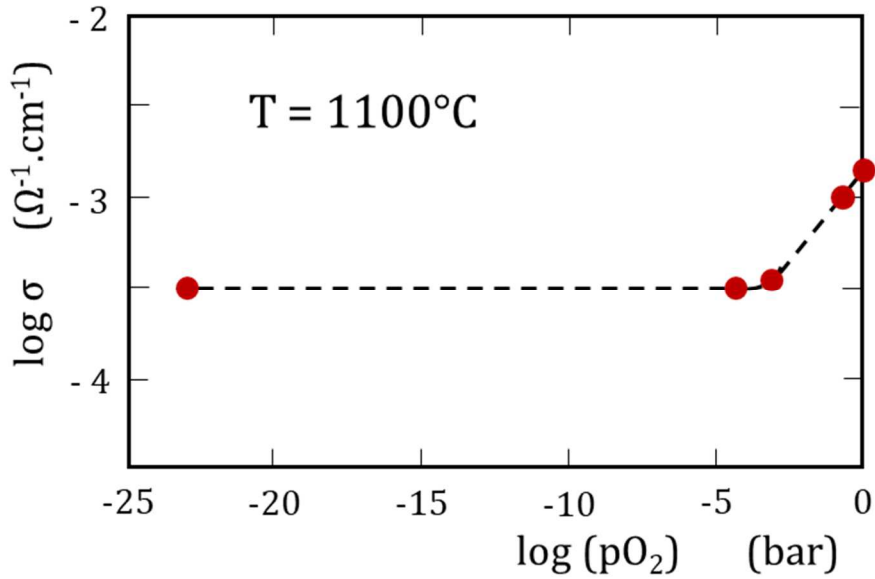


Figure 10: Patterson diagram of the HZFC refractory, at 1100°C.

It should be pointed out that, with the composite material studied, the pressure independent plateau, ascribed to ionic conductivity is a contribution of both the zirconia and the vitreous phases. The vitreous phase is an alumino-silicate compound which is either an insulator or an ionic conductor by cation. Thus, the mixed ionic-electronic conductivity can be ascribed to the zirconia phase. Various authors have demonstrated that monoclinic zirconia is a mixed ionic-electronic conductor, with predominant electronic conductivity [27–30]. Consequently, according to the slowness rule [21], the semipermeation flux is controlled by the anionic defects which are the minority carriers (see Section 3.3).

### 3.3. Blistering vs. oxygen semipermeability

The oxidized refractory was tested in the semipermeability set-up described in Figure 1. Air was flowing in the lower chamber of the cell and pure Argon (oxygen partial pressure of the order of  $10^{-6}$  bar) in the upper chamber. As it will be shown hereafter, in case of blistering within a glass melt, the oxygen content downstream the cell was, generally, of a few

hundred ppm or even more, compared with less than 10 ppm with a gas/refractory/gas configuration, which corresponds to a very low oxygen permeation flux (Table 1). According to previous studies, this low oxygen flux can be ascribed to a polarization phenomenon at the lean side of the surface of the membrane [31, 32].

Table 1: Oxygen content (in ppm) in flowing argon downstream the semipermeability cell as a function of temperature (gas | refractory | gas configuration).

$T_{\text{pellet}} \text{ (}^\circ\text{C)}$	Oxygen content, downstream the cell (ppm)
1127	5.4
1227	7.2
1328	10.8

The modified set-up involving a refractory crucible, shown in Figure 2, was used instead of the standard pellet, and the crucible was filled with glass. The variation with time of the oxygen content in flowing argon, downstream the cell, at 1100°C, starting with a raw refractory crucible is given in Figure 11. The sensor emf was recorded continuously and a calculation of the oxygen pressure and then of the oxygen flow was made every second (Figure 11 (a)). Figure 11 (b) was obtained by integration over one hour of the oxygen evolving from the glass melt.

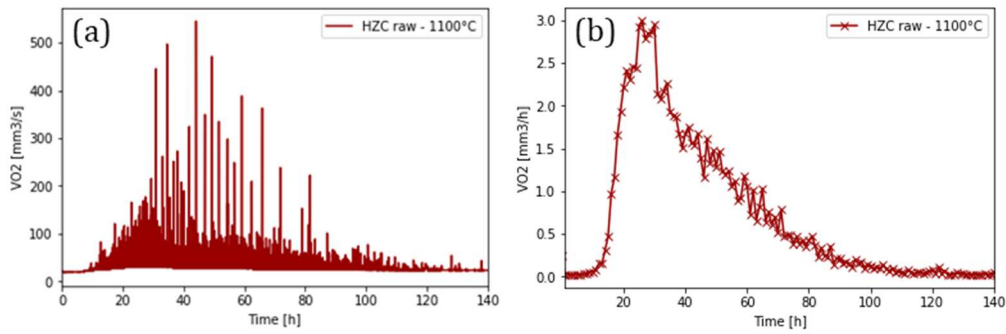


Figure 11: Blistering phenomenon at 1100°C of a glass in contact with a raw refractory –  $p_{O_2(\text{rich})} = 0.2$  bar.

(a) Instantaneous oxygen volume, (b) integration of the blistering oxygen volume over one hour

It should be pointed out that the basis line was always lower than 10 ppm indicating the high gas-tightness of the set-up. Each peak observed in Figure 11 (a) corresponds to the oxygen released by a bubble (or a few bubbles) when it explodes. It is also noted in Figure 11 (b) that the blistering process started only after 13 hours experiment with a raw refractory. The comparison of this incubation time is given in Figure 12: with a raw refractory, the incubation time before blistering start was 13 hours (Figure 12 (a)) while it was only two hours with a previously oxidized crucible (1350°C, 30 hours under air) (Figure 12 (b)). The longer incubation time observed with the raw refractory can be ascribed to the presence of metallic iron. As long as all metallic iron present in the raw refractory is not fully oxidized to iron (II) or (III), according to the proposed mechanism previously described, the oxygen entering the refractory from the oxygen-rich side is consumed. Fe(II) is being oxidized, as long as the Fe(II)/Fe(III) equilibrium is not reached. Then, oxide ions cannot reach the glass/refractory interface, and, consequently the blistering cannot start.

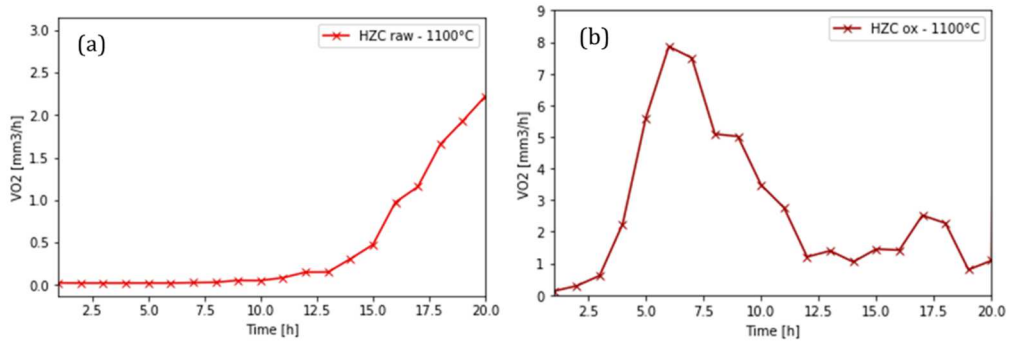


Figure 12: Blistering of the tested glass in contact with a raw (a) and oxidized (b) HZC refractory –  $p_{O_2} = 0.2$  bar, at  $1100^{\circ}\text{C}$ .

Various experiments were carried out to precise the key parameters of the blistering process. As the semipermeability measurements were characterized by an oxygen zirconia sensor, only the oxygen mole fraction within the bubbles was measured and it was not possible to ensure that the gas contained in bubbles is only oxygen. For analysing the various components of the permeating gas, a mass spectrometer was added downstream the oxygen sensor. As shown in Figure 13, negligible nitrogen content was detected within the produced bubbles. This result confirms that the permeation flux is not a physical one through the open porosity or micro-cracks of the pellet but an electrochemical semipermeability across the zirconia phase.

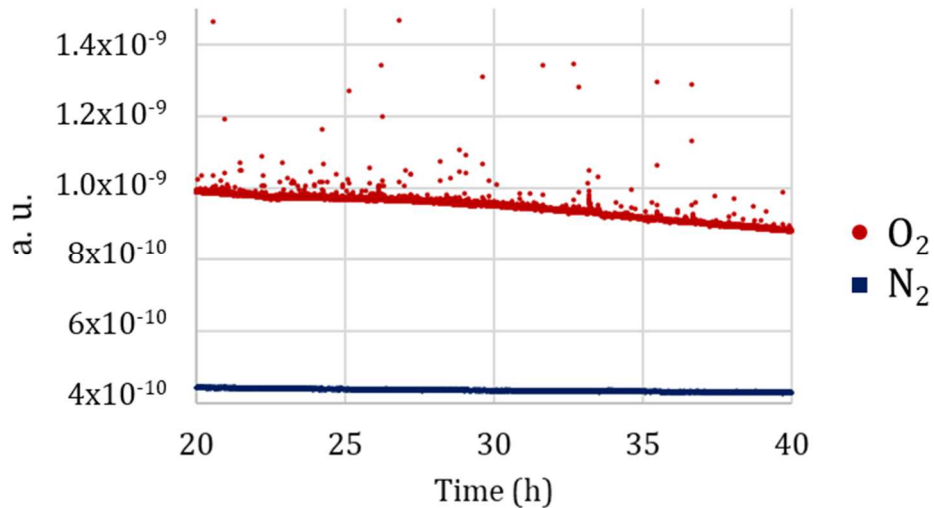


Figure 13: Mass spectrometer analysis of the gases released by the bubble explosion of HZC tested at 1100°C in the semipermeability set-up ( $pO_2 = 0.2$  bar)

To visualize the blistering phenomenon, a sessile drop design was used [33]. A piece of glass on a refractory pellet is melted in a horizontal tubular resistance furnace. The vessel is a high-purity gas-tight alumina tube with water-cooled seals. An alumina holder, sliding inside the alumina tube, allows to set the sample in the center of the furnace. The temperature of the sample is determined with a Pt-Pt (10 %) Rh thermocouple located under it. Two windows at each side of the tube allow the drop to be illuminated and its shadow to be observed on a camera (monochrome camera BASLER CMOS 2/3 35i/s). An example of observation of bubble formation within a glass droplet at the interface with an oxidized refractory pellet is shown in Figure 14. Air was flowing around the glass drop. At the interface glass/refractory the oxygen activity is low. Consequently, an oxygen activity gradient is established between the center of the drop and its periphery. The situation resembles the corrosion by differential aeration observed for a drop of water under air, placed on a steel plate: the oxidation occurs in the center of the drop [34, 35]. The situation can also be compared to the semipermeability set-up shown in Figure 2. The photographs demonstrate that the time necessary for a bubble to be formed at the glass/refractory interface, to go up till the surface, and to blast, liberating

oxygen which is measured by the oxygen sensor, requires one hour, or more, according to the temperature and the height of glass on the refractory. This time can be compared to the incubation time observed with oxidized refractories (Figure 12 (b)).

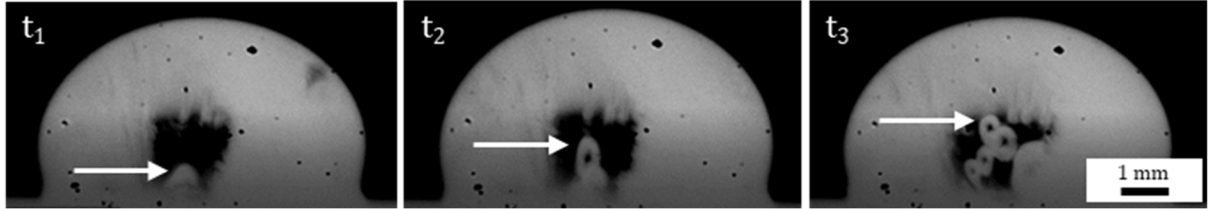


Figure 14: Bubble rise within a glass droplet, at 1100°C, under air atmosphere, at  $t_1 = 0$  min,  $t_2 = 10$  min, and  $t_3 = 25$  min

The role of the oxygen-rich atmosphere on the blistering phenomenon was demonstrated by a sharp lowering of the partial pressure of oxygen at the rich side ( $P_3$ ): when the oxygen partial pressure was changed from  $pO_2 = 0.2$  bar down to  $pO_2 = 10^{-5}$  bar (in argon) the blistering decreases and disappears after a while. However, the blistering switch-off is not instantaneous after lowering the  $pO_2$  since bubbles already formed in the glass are still growing and rising up in the glass until they burst. As explained before, the time is dependent on the glass viscosity. Once the blistering phenomenon is completely stopped it can start again while increasing again the oxygen partial pressure at the rich side of the semipermeability set-up.

The role of temperature on the blistering phenomenon is complex because the molten glass and the refractory are concerned [36]. According to Wagner's theory, assuming that bulk diffusion within the refractory is the rate limiting process, the oxygen semipermeation flux is proportional to the ambipolar conductivity  $\sigma_{amb}$  [37-39]:

$$J_{O_2} = \frac{1}{4^2 F^2 L} \int_{\mu_{O_2}^{lean}}^{\mu_{O_2}^{rich}} \sigma_{amb} d\mu_{O_2} \quad (3)$$

where,

- L: thickness of the membrane

- $\mu_{O_2}^{lean}$ : oxygen chemical potential on the lean side of the refractory
- $\mu_{O_2}^{rich}$ : chemical potential on the rich side of the refractory
- $\sigma_{amb}$ : ambipolar conductivity which is defined as  $\sigma_{amb} = \frac{\sigma_i \sigma_e}{\sigma_i + \sigma_e}$
- $\sigma_i$  and  $\sigma_e$  are the ionic and electronic conductivity

In case of an oxide in which the ionic conductivity  $\sigma_i$  is predominant (referred to as “solid electrolyte”) the ambipolar conductivity can be approximated as  $\sigma_e$ ; on the contrary, for a semi-conductor ( $\sigma_i \ll \sigma_e$ ), the ambipolar conductivity can be reduced to  $\sigma_i$ . Consequently, according to Wagner’s theory, the semipermeation flux is governed by the minority charge carriers. It should be noted that many steps have to be considered in the permeation process, i.e., gas transfer to and from the gas/solid interface, oxygen exchange at both interfaces of the membrane, etc. [39]. It is not the aim of this work to recall in detail all the steps of the process.

The ambipolar conductivity, and consequently, the permeation flux increases exponentially with temperature. Figure 15 compares the blistering phenomenon with a raw refractory, at 1050°C and 1100°C, respectively. The results show that the incubation time is noticeably lower at 1100°C than at 1050°C: 14 hours and more than 35 hours, respectively. The oxygen flux being noticeably higher at 1100°C, the oxidation of metallic iron particles within the refractory are oxidized more rapidly than at 1050°C, consequently, the blistering phenomenon starts more rapidly. Obviously, as shown in Figure 15, the blistering is also more intense at high temperature.

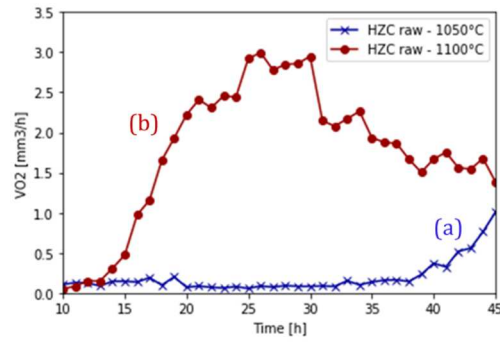


Figure 15: Semipermeability experiments at two temperatures with raw HZFC refractory: (a) 1050°C, (b) 1100°C

Considering that the density of the bubble is very low compared to the density of the molten glass ( $\rho_{\text{glass}} \gg \rho_{\text{gas}}$ ), the expression for the rising velocity of a bubble in a viscous liquid, called the Hadamard-Rybczynski velocity,  $v_{HR}$  is [40, 41]:

$$v_{HR} = \frac{\rho_{\text{glass}} g r^2}{3 \mu_{\text{glass}}} \quad (4)$$

where  $\rho_{\text{glass}}$  and  $\mu_{\text{glass}}$  are the glass density and the glass viscosity, respectively,  $g$  is the gravitational acceleration, and  $r$  the bubble radius.

According to equation (4), the higher the bubble size, the higher the rising rate. Moreover, the glass properties play an important role in the blistering process, and, mainly, the glass viscosity which decreases exponentially with temperature [42]. Consequently, the rising velocity of the bubbles increases, and the incubation time with an oxidized refractory decreases, as the temperature increases.

#### 4. Conclusion

This work demonstrates for the first time the role of the oxygen semipermeation process through refractory in the blistering process, in the case of a high zirconia fused-cast refractory below the allotropic transformation of zirconia, owing to the connectivity of the zirconia phase. The vitreous phase only plays a mechanical role, allowing the refractory to withstand the monoclinic-tetragonal phase transformation without cracking both on heating and cooling. The study also demonstrates the role of refractory iron oxidation state, and of temperature, on the delayed initiation of the blistering mechanism. These results are also important from an industrial point of view because they make it possible to provide ways for reducing or even canceling the phenomenon of blistering.

### **Acknowledgements**

Saint-Gobain Research Provence is acknowledged for financial support of this work.

J. Durst and S. Brossard (Saint-Gobain Research Centre Paris) are acknowledged for assistance in the XANES experiments. S. Coindeau and L. Salvo (SIMAP, Grenoble) are acknowledged for assistance in the interpretation of the X-ray absorption tomography experiments. XRD characterizations and SEM observations were carried in the Consortium des Moyens Technologiques Communs (CMTC) of Grenoble-INP.

### **References**

- [1] V. Gottardi, Refractories for the glass industry. *J. Non-Cryst. Solids*, 80(1-3) (1986) 93–102.
- [2] P. Epicoco, B. Coasne, A. Gioia, P. Papet, I. Cabodi, M. Gaubil, Mesoscopic Monte Carlo simulations of microstructure and conductivity of ZrO<sub>2</sub>–glass composites, *Acta Materialia*, 61 (2013) 5018–5025.

- [3] F. G. K. Baucke, G. Röth, Electrochemical mechanism of the oxygen bubble formation at the interface between oxidic melts and zirconium silicate refractories, *Glastechnische Ber.-Glass Sci. Technol.* 61(5) (1988) 109–118.
- [4] F. W. Kramer, Analysis of Gases Evolved by AZS Refractories and by Refractory Glass Melt Reactions – Techniques and Results – Contribution to the Bubble-Forming Mechanism of AZS Material, *Glastechnische Ber.-Glass Sci. Technol.* 65(4) (1992) 93–98.
- [5] F. A. G. van Dijk, Glass defects originating from glass melt/fused cast AZS refractory interaction, PhD Thesis, Technol. Univ. Eindhoven, 1994. <https://doi.org/10.6100/IR417346>.
- [6] *Electrochemistry of Glasses and Glass Melts, Including Glass Electrodes*, H. Bach, F.G.K. Baucke, D. Krause, Eds., 2001, Springer Verlag, Berlin.
- [7] K. Madi, S. Forest, M. Boussuge, S. Gailliègue, E. Lataste J. Y. Buffiere, D. Bernard, D. Jeulin, *Comput. Mater. Sci.*, 39 (2007) 224-229.
- [8] L. Petroni, Michel Boussuge, D. Ryckelynck, Numerical simulation of the cooling-down of high-zirconia fused-cast refractories, *J. Europ. Ceram. Soc.*, 32 (2012) 3941–3947.
- [9] J. Poirier, E. Blond, E. de Bilbao, R. Michel, A. Coulon, J. Gillibert, M. Boussuge, Y. Zhang, D. Ryckelynck, G. Dusserre, T. Cutard, P. Leplay, New advances in the laboratory characterization of refractories: testing and modelling, *Metall. Res. Technol.*, 114 (2017) 610.
- [10] B. Ravel, M. Newville, ATHENA, ARTEMIS, HEPHAESTUS: data analysis for X-ray absorption spectroscopy using IFEFFIT, *J. Synchrotron Radiation*, 12(4) (2005) 537–541.
- [11] A. Caneiro, M. Bonnat, J. Fouletier, Measurement and regulation of oxygen content in selected gases using solid electrolyte cells. IV. Accurate preparation of CO<sub>2</sub>-CO and H<sub>2</sub>O-H<sub>2</sub> mixtures, *J. Appl. Electrochem.*, 11 (1981) 83–90.
- [12] J. Fouletier, E. Siebert, A. Caneiro, Accurate monitoring of low oxygen activity in gases with conventional oxygen gauges and pumps, in: *Science and Technology of Zirconia II*, Adv.

In Ceram., Vol. 12, N. Claussen et al. (Eds.), Am. Ceram. Soc., Columbus, 1984, pp. 618–626.

[13] J. Fouletier, P. Fabry, M. Kleitz, Electrochemical semipermeability and the electrode microsystem in solid oxide electrolyte cells, *J. Electrochem. Soc.* 123 (1976) 204–213.

[14] M. Guillodo, J. Fouletier, L. Dessemond, P. Del Gallo, Oxygen Permeation Through Dense  $\text{Bi}_2\text{V}_{0.9}\text{Cu}_{0.1}\text{O}_{5.35}$  Ceramic Membranes, *J. Electrochem. Soc.*, 149 (2002) J93–J99.

[15] P. M. Geffroy, A. Vivet, J. Fouletier, N. Richet, P. Del Gallo, T. Chartier, Influence of Oxygen Surface Exchanges on Oxygen Semipermeation through  $\text{La}_{(1-x)}\text{Sr}_x\text{Fe}_{(1-y)}\text{Ga}_y\text{O}_{3-\square}$  Dense Membrane, *J. Electrochem. Soc.*, 158 (8) (2011) B971–B979.

[16] C. Salles, J. Fouletier, D. Marinha, M. C. Steil, Determining the rate-limiting step during oxygen semipermeation of  $\text{CaTi}_{0.9}\text{Fe}_{0.1}\text{O}_{3.8}$  oxygen transport membranes, *J. Membr. Sci.* 527 (2017) 191–197.

[17] P. M. Geffroy, A. Vivet, J. Fouletier, C. Steil, E. Blond, N. Richet, P. Del Gallo, T. Chartier, The Impact of Experimental Factors on Oxygen Semipermeation Measurements, *J. Electrochem. Soc.*, 160 (1) (2013) F60–F68.

[18] P. M. Geffroy, E. Deronzier, J. Gillibert, P. Munch, T. Chartier, J. Fouletier Determination of Oxygen Diffusion and Surface Exchange Coefficients of Mixed Ionic-Electronic Conductors by Oxygen Semipermeation Methods, *J. Electrochem. Soc.*, 167 (2020) 064503.

[19] J. Fouletier, E. Mantel, M. Kleitz, Performance characteristics of conventional oxygen gauges, *Solid State Ionics.* 6 (1982) 1–13.

[20] J. Fouletier, E. Siebert, A. Caneiro, Accurate monitoring of low oxygen activity in gases with conventional oxygen gauges and pumps, in: *Sci. Technol. Zirconia II*, N. Claussen, M. Ruhle, A.H. Heuer, Am. Ceram. Soc. Inc., Columbus, OH (USA), 1983, pp. 618–626.

- [21] P. Sarrazin, A. Galerie, J. Fouletier, *Mechanisms of High Temperature Corrosion: a Kinetic Approach*, Trans. Tech. Publ. Ltd, Zürich, Switzerland, 2008.
- [22] J. W. Patterson, E. C. Bogren, R. A. Rapp, Mixed conduction in  $Zr_{0.85}Ca_{0.15}O_{1.85}$  and  $Th_{0.85}Y_{0.15}O_{1.925}$  solid electrolytes, *J. Electrochem. Soc.*, 114 (7) (1967) 752–758.
- [23] J. W. Patterson, Conduction Domains for Solid Electrolytes, *J. Electrochem. Soc.*, 118 (7) (1971) 1033–1039.
- [24] D. L. Douglass, C. Wagner, Oxidation of Oxygen-Deficient Zirconia and its Relationship to the Oxidation of Zirconium, *J. Electrochem. Soc.*, 113 (7) (1966) 671–76.
- [25] P. J. Harrop, J. N. Wanklyn, On the Defect Structure of  $ZrO_2$  and  $HfO_2$ , *J. Electrochem. Soc.*, 110 (12) (1963) 1285.
- [26] P. Kofstad, Effect of Impurities on the Defects in Oxides and Their Relationship to Oxidation of Metal, *Corrosion-Nace* 24 (1968) 379–388.
- [27] R. W. Vest, N. M. Tallan, W. C. Tripp, Electrical properties and defect structure of zirconia: I, monoclinic phase, *J. Am. Ceram. Soc.*, 47 (12) (1964) 635–640.
- [28] A. Madeyski, W. W. Smelzer, Oxygen diffusion in monoclinic zirconia, *Mat. Res. Bull.*, 3 (4) (1968) 369–375.
- [29] N. M. Nasrallah, D. L. Douglass, Ionic and electronic conductivity in  $Y_2O_3$ -doped monoclinic  $ZrO_2$ , *J. Electrochem. Soc.*, 121(2) (1974) 255–262.
- [30] O. H. Kwon, C. Jang, J. Lee, H. Y. Jeong, Y-i. Kwon, J. H. Joo, Investigation of the electrical conductivity of sintered monoclinic zirconia ( $ZrO_2$ ), *Ceram. Int.*, 43 (11) (2017) 8236–8245.
- [31] M.C. Steil, J. Fouletier, P.-M. Geffroy, Surface exchange polarization vs. gas concentration polarization in permeation through mixed ionic-electronic membrane, *J. Membr. Sci.* 541 (2017) 457-464

- [32] A. Riffaud, Oxygen semipermeability and conductivity characterization of ceramics, Internal report, SGR-Cavaillon, RE 2427, 2017.
- [33] D. Chatain, F. Chabert, V. Ghetta, J. Fouletier, New Experimental Setup for Wettability Characterization under Monitored Oxygen Activity: I, Role of Oxidation State and Defect Concentration on Oxide Wettability by Gold, *J. Am. Ceram. Soc.*, 76 (6) (1993) 1568–1576.
- [34] J. O'M. Bockris, A.K.N. Reddy, *Modern Electrochemistry*, vol. 2, Plenum, New York, 1970, pp. 1301–1305.
- [35] U. R. Evans, *The Corrosion of Metals*, Arnold, London, 1926, p. 93.
- [36] H. Kočárková, *Stability of glass foams: experiments at the bubble scale and on vertical film*, PhD Thesis, Paris Est, 2011.
- [37] H. J. M. Bouwmeester, H. Kruidhof, A. J. Burggraaf, *Solid State Ionics*, 72 (Part 2) (1994) 185–194.
- [38] Y.S. Lin, W. Wang, J. Han, Oxygen permeation through thin mixed-conducting solid oxide membranes, *AIChE J.*, 40 (5) (1994) 786–798.
- [39] C. Li, J. J. Chew, A. Mahmoud, S. Liu, J. Sunarso, Modelling of oxygen transport through mixed ionic-electronic conducting (MIEC) ceramic-based membranes: An overview, *J. Membr. Sci.*, 567 (2018) 228–260.
- [40] J. S. Hadamard, Mouvement permanent lent d'une sphère liquide et visqueuse dans un liquide, *C. R. Acad. Sci.*, 152 (1911) 1735–1738 (in French).
- [41] W. Rybczynski, Über die fortschreitende Bewegung einer flüssigen Kugel in einem zähen Medium, *Bull. Acad. Sci. Cracovie A1* (1911) 40–46 (in German).
- [42] R. G. C. Beerkens, H. de Waal, *Handbook for Glass Technologists*, TNO-TPD Glass Technology. Eindhoven, 1997.